Journal of Electroanalytical Chemistry 882 (2021) 115024

Contents lists available at ScienceDirect

Journal of Electroanalytical Chemistry

journal homepage: www.elsevier.com/locate/jelechem

Electrolytic co-deposition neutron production measured by bubble detectors

Phillip J. Smith *, Robert C. Hendricks, Bruce M. Steinetz

National Aeronautics and Space Administration, John H. Glenn Research Center, 21000 Brookpark Road, M.S. 302-1, Cleveland, OH 44135, United States

ARTICLE INFO

Article history:
Received 2 October 2020
Received in revised form 14 January 2021
Accepted 15 January 2021
Available online 19 January 2021

Keywords:
Co-deposition
Palladium
Deuterium
Neutron
Dosimetry
Dendrite

ABSTRACT

Co-deposition electrochemical cells are a simple means to examine novel nuclear reactions. In this study, palladium and deuterium atoms were co-deposited on a cathode at stoichiometric densities, forming dendritic morphologies. Bubble detector neutron dosimeters were used to measure equivalent dose levels during electrolytic deposition. Cells expected to produce excess neutrons were denoted as experimental cells and contained an electrolyte consisting of palladium(II) chloride, lithium chloride, and heavy water. The control cells used copper(II) chloride, lithium chloride, and heavy water electrolyte. Thirteen experimental and nine control cells were supplied current, increasing from 0.1 to 100.0 mA over a period of 20 days. Neutron radiation levels detected near experimental cells were, on average, greater than those measured near control cells for the entire test profile. For test days 9 through 20, the experimental cells exhibited significantly higher average neutron radiation than the controls at a 99% confidence level.

1. Introduction

In the field of low-energy nuclear reactions (LENR), anomalous heat production and measurement remains a highly controversial subject. No commonly accepted explanations for LENR exist, and positive result claims are often found to be difficult to replicate [1,2]. There is even controversy whether nuclear processes are involved. It has been suggested that nuclear particle detection may be a preferred identification method, as opposed to measuring momentary thermal anomalies [3]. Thus, to accumulate evidence that unexpected nuclear chemistry is occurring, daily neutron emissions were monitored using a protocol presumed to exhibit atypical nuclear chemistry properties.

The nuclear chemistry sources employed here are electrolytic co-deposition cells, which are similar to those developed by Mosier-Boss et al. [4–6], implemented by Tanzella et al. [7], and reported in many other instances. This co-deposition protocol appears to build the cathode morphology required to trigger the reactions of interest, such as those generating fast neutrons. Comparable electrochemical experiments have resulted in sustained observations of tritium production [3,8]. As such, it is of interest to monitor potential neutron activity throughout the course of the experiment.

Dosimeters are a class of devices used to measure ionizing radiation. Many forms of personal dosimeters exist to monitor levels of whole-body equivalent doses. Bubble detectors, in particular, measure neutron doses via superheated liquid droplets distributed throughout a transparent polymer media [9,10]. If a neutron having more than 200 keV energy impinges on a droplet, then the superheated liquid droplet expands and becomes a visible gas bubble.

Bubble detector dosimeters are commonly used in a variety of industrial, medical, and research applications, including the International Space Station [11,12]. The bubble detectors are of comparable size to the electrolysis cells and have been previously used for fast-neutron detection near co-deposition cells [13]. Additionally, these dosimeters enable equivalent dose measurement at any time by visually inspecting and counting the number of bubbles. In previous iterations, co-deposition-generated radiation was often only recorded by Columbia Resin 39 (CR-39) plastic chips, which require cell disassembly to access, preparation to analyze, and significant effort to manually count nuclear tracks.

The purpose of these experiments was to evaluate bubble detectors as real-time dosimeters monitoring the co-deposition process, compare cumulative radiation doses detected near cells with two distinct electrolytic compositions, determine if there are neutron emissions above background levels, show that cells of this chemistry are safe to operate, and review factors that may affect neutron generation.

Abbreviations: AD, Anderson-Darling; *b*, number of bubbles in the bubble detector; C, control; CR-39, Columbia Resin 39; $CuCl_2$, copper chloride; D, deuterium, deuteride; D_20, heavy water; DI, de-ionized; E, experimental; *H*, equivalent dose; HNO_3, nitric acid; HPGe, high-purity germanium gamma detector; LENR, low-energy nuclear reaction; LiCl, lithium chloride; OSHA, Occupational Health and Safety Administration; p, *p*-value; $PdCl_2$, palladium chloride; *S*, manufacturer quoted calibrated detector sensitivity in bubbles per μSv; SA, Sigma-Aldrich; T, trial.

* Corresponding author.
E-mail addresses: phillip.j.smith@nasa.gov (P.J. Smith), robert.c.hendricks@nasa.gov (R.C. Hendricks), bruce.m.steinetz@nasa.gov (B.M. Steinetz).

http://dx.doi.org/10.1016/j.jelechem.2021.115024

2. Experimental methods and materials

2.1. List of materials

Test materials were de-ionized (DI) water, Cambridge Isotope Laboratories heavy water (D_2O), Sigma-Aldrich (SA) palladium(II) chloride ($PdCl_2$), SA copper(II) chloride ($CuCl_2$), SA lithium chloride (LiCl), SA nitric acid (HNO_3), SA 0.25-mm-diameter gold wire, and SA 0.25-mm-diameter platinum wire.

2.2. Electrolysis cell assembly

A test system diagram is shown in Fig. 1, including electrical circuits and a detailed view of the electrolysis cell interior. The electrodes were placed on opposite sides of the cell, and each were secured on a plastic mesh lattice. A spacer was cut from a polyethylene sheet (approximately 1.3 cm wide and 2.5 cm long) to keep the electrodes upright and prevent contact between them. The platinum and gold wires, each greater than 99.9% purity on a trace metals basis, were cut to lengths of ~ 22 cm for the platinum anode and ~ 13 cm for the gold cathode. For cleaning, the electrode wires were immersed in a ~ 2 M nitric acid solution for several minutes then rinsed by placing them in a beaker with DI water. All plastic components and two glass capillary tubes were thoroughly rinsed with DI water. These materials were left to dry completely in air.

The plastic mesh lattice pieces were used to support the electrode wires. The clean platinum wire was passed through the plastic lattice as appears in Fig. 2(a). The gold wires were placed on the lattice as shown in Fig. 2(b). Blue CR-39 solid state nuclear track detector chips were also attached to this cathode lattice construction but were not used for reaction analysis in this effort.

The two lattice pieces retaining the electrode wires were placed into the acrylic cell. These two lattices were pressed apart by the polyethylene spacer that was bent to fit in between the electrodes, resulting in a nominal cathode-to-anode spacing of 2 cm. The acrylic cell cover was placed on top of the cell, and the electrode wires were positioned through pre-drilled holes. Glass capillary tubes were inserted into the remaining two small holes in the cover for protection of and to prevent contamination from thermocouple probes. The desired electrolyte solution was transferred by pipet into the acrylic cell through a center hole, and the initial fluid level was marked on the side of the cell before the unit was transferred to a fume hood, placed in a clamp, and loosely surrounded with silicone insulation to allow better grip with the clamp. This volume of electrolyte submerged approximately 9 cm of gold wire and 18 cm of platinum wire. Once secured by the clamp, the appropriate electrical supply and monitoring leads were attached to the electrode wires.

In this publication, cells that include $PdCl_2$ in the electrolyte are denoted as experimental cells. The cells with $CuCl_2$ are control cells. The desired concentration of the experimental cell electrolyte solution was 0.03 M $PdCl_2$ and 0.3 M LiCl in D_2O, as used in previously reported co-deposition investigations [4–6,13,14]. For a control cell, the desired electrolyte concentration was 0.03 M $CuCl_2$ and 0.3 M LiCl in D_2O. The LiCl is desired to support dissolution of the primary metallic salt.

Bubble Technology Industries Personal Neutron Dosimeters were used for neutron detection and placed behind the cells, midway between the

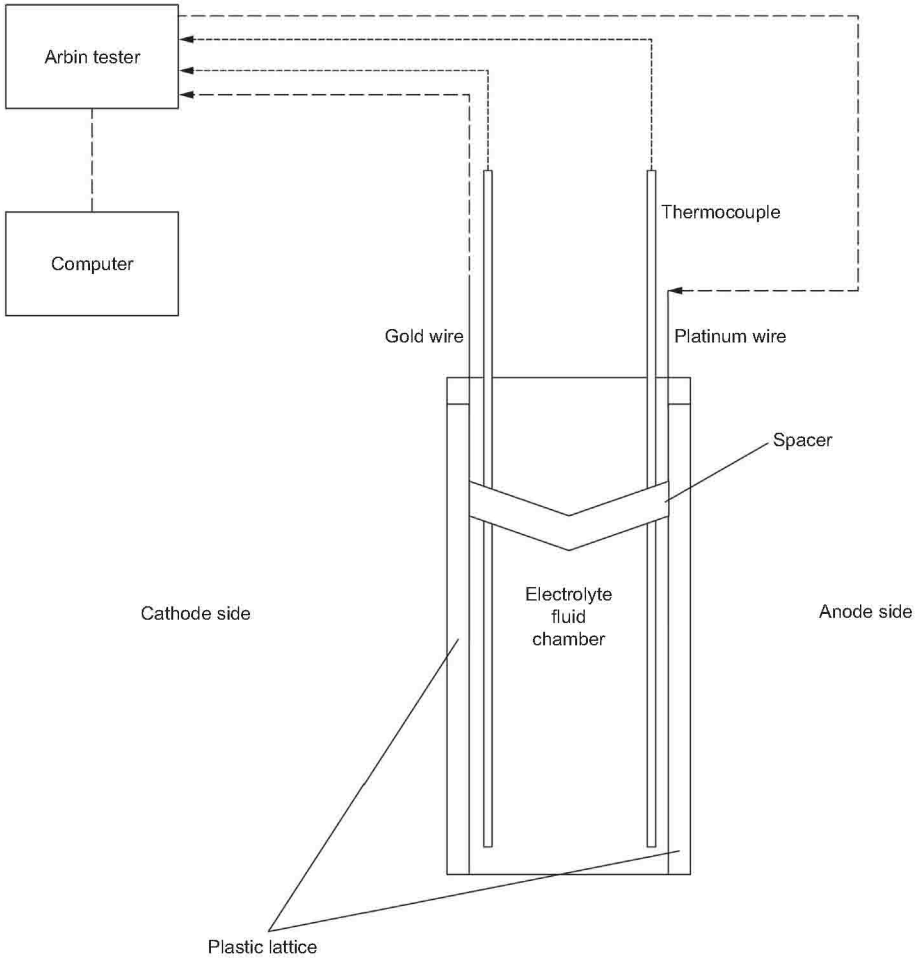

Fig. 1. Test system diagram for a single electrolysis cell. A single bubble detector was placed outside the cell behind the electrolyte chamber as shown in this view.

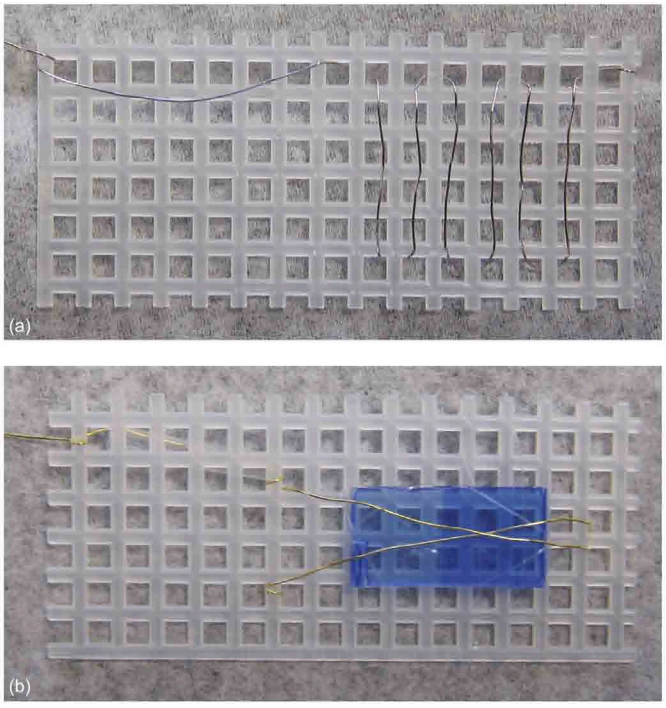

Fig. 2. (a) Platinum anode wire wrapped so there are six horizontal crossings on the lattice. (b) Gold cathode wire arranged in a"V" shape and secured to the lattice over a Columbia Resin 39 solid-state nuclear track detector (results not reported here).

electrodes with the cathode always to the left, as is shown in Fig. 3. These dosimeters were calibrated for sensitivity within the range of 0.88 to 3.2 bubbles per μSv [8]. Detectors were capped and reset between periods of usage.

Cell current was controlled using an Arbin BT-2000 battery tester programmed to supply the current profile exhibited in Table 1. This instrument was chosen for the capability to provide desired currents up to 100 mA with ±0.1% accuracy and to monitor voltage with a sensitivity of ±100 mV. The current direction from anode to cathode promotes co-deposition of palladium and deuterium onto the gold cathode in experimental cells and co-deposition of copper and deuterium in control cells. The current profile durations and magnitudes are based on a known successful charging profile to promote adherence [5,6,15]. In order to obtain statistically useful

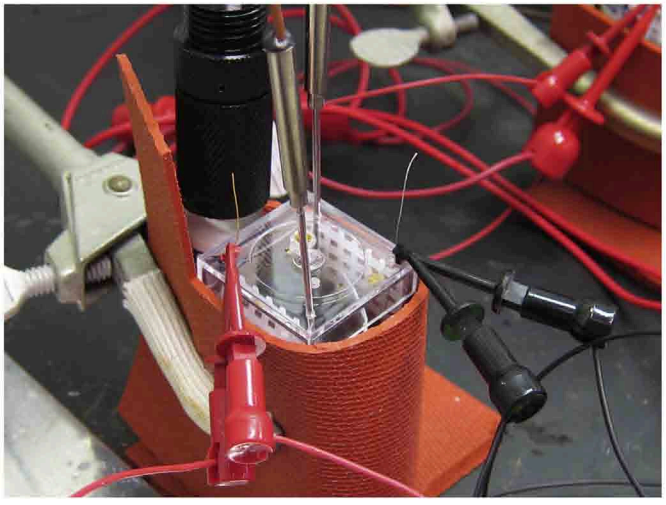

Fig. 3. A cell as it appears when completely assembled with the gold cathode (left) and platinum anode (right) wires visible. The bubble detector is securely placed behind the cell.

Table 1
Current-Time Profile for Cell Electrolysis.

Step	Duration, hours:minutes	Current, mA
1	0:05	0.0
2	24:00	0.1
3	24:00	0.2
4	284:00	0.5
5	24:00	5.0
6	24:00	10.0
7	24:00	25.0
8	24:00	50.0
9	≥24:00	100.0
10	0:05	0.0

 Note: The duration of Step 9 was often extended to postpone completion of a trial.

information regarding cell performance, it was beyond the scope of this project to fully evaluate multiple current profiles. The most important aspect of the profile is to, initially, keep current low so that metals in solution (Pd and Cu) plate out and attach to the gold cathode. Considering the submerged length of cathode wire, the current density ranges from 0.14 mA·cm^{-2} in Step 2 to 140 mA·cm^{-2} in Step 9. The anodic current density is approximately half the cathodic current density.

Cells were given names in the following form: Trial (T)-Roman numeral-Cell type (E for Experimental or C for Control) and Arabic numeral. For example, the third Experimental cell of Trial IV is denoted as T-IV-E3. If there existed only one cell of a particular type in a Trial, the final number is omitted. All experimental and control cells contained the same previously described electrolyte solutions and were operated at room temperature inside of a fume hood.

Bubble detectors were visually counted once per day for bubbles appearing between the rounded dosimeter bottom and the start of a sticker label located midway across the unit. For reference, Fig. 4 shows many bubbles dispersed throughout the bubble detector polymer media. Additional cell maintenance consisted of daily visual inspections of electrical connections and additions of pure heavy water to maintain the initial fluid level to ensure the electrodes remained sufficiently submerged, since the cells were of an open, unpressurized design that allowed normal evaporation.

3. Data analysis

The equivalent dose detected near each cell was defined as

$$H = \frac{b}{S} \tag{1}$$

where b is the total number of bubbles in the detector tube and S is the manufacturer-calibrated detector sensitivity in bubbles per micro-Sievert.

Fig. 4. Bubble Detector Personal Neutron Dosimeters. Neutron-induced bubbles are visible in these three uncapped and used bubble detectors. Polymer detection media is the translucent section to the left of the white label, which displays the serial number and calibration data for each detector.

Daily averages and sample standard deviations were calculated for experimental cells as a set, and then for control cells as a separate set. Anderson-Darling (AD) tests were conducted to evaluate the data distribution normality and the appropriateness of further statistical treatments [16]. Calculated AD values were less than the AD critical value, indicating that there was insufficient evidence to reject the null hypothesis that the sample data were normally distributed. Therefore, subsequent analyses considered the data to be normally distributed.

Confidence intervals were calculated for the 95% confidence level using a Student's *t*-test. For days during a test without a bubble detector reading, total bubble counts were linearly interpolated between data recordings for the purposes of calculating averages and confidence intervals. Differences in the mean values between experimental and control cells were evaluated using a two-tailed Welch's unequal variance t-test, with the null hypothesis being that the means were equal. This test was selected because of the unequal sample sizes in the experiment and control populations.

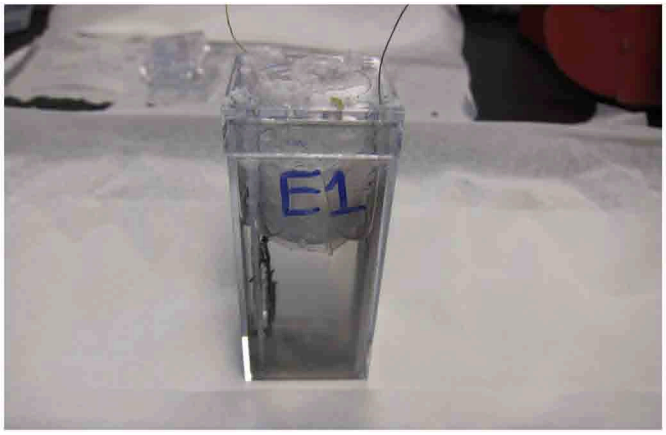

Fig. 6. Exterior of T-III-E1 prior to post-test disassembly, showing a colorless and nearly clear electrolyte solution.

4. Results

4.1. Cell operation and observations

Cell voltage, as a function of applied current, was used as a cell health and electrical continuity metric. Fig. 5 shows the typical voltage response to the current-time profile for several experimental and control cells. Following the plating phase during the first three steps, the measured voltage profiles were consistent between cells and between trials. Earlier in the profile, the control cells exhibited more variability. The occasional sudden voltage drops are indicators of when the electrolyte fluid was replenished by adding pure heavy water. Although electrolyte temperature was monitored for each cell, no temperature differences were observed between experimental and control cells when using type K thermocouples that typically provide accuracy to ±2.2 °C.

In Fig. 6, it is shown that the electrolyte solution was colorless and nearly clear following the electrolytic protocol. Both experimental and control cells, which were amber and blue, respectively, prior to applying current, appeared similarly clear following testing. This is evidence that most of the initial salt cations were removed from solution by the current-time protocol.

4.2. Radiation measurements

In total, 13 experimental cells and 9 control cells completed the entire current-time profile in the standard test configuration previously described. No cells constructed and operated in this standard configuration were omitted from the presented results. Average radiation levels detected for both cell groups are reported in Fig. 7. Radiation levels detected near the experimental cells are, on average, greater than that measured near the control cells for the entirety of the test profile from test start to the end of the current-time profile. The upper and lower 95% confidence intervals are presented for the average cumulative radiation dose per cell, calculated for the experimental cells and the control cells as separate groups without pooling the variances. This visually presents the statistically significant separation in neutron emissions between the experimental and control cells. The lower 95% confidence interval limit of the experimental cell is greater than the upper 95% confidence interval limit of the control cell from test days 9 through 20. Additionally, for the same test day range, the Welch's *t*-test shows that there is significantly more average cumulative radiation detected near experimental cells compared with that from control cells at a 99% confidence level ($p < 0.01$).

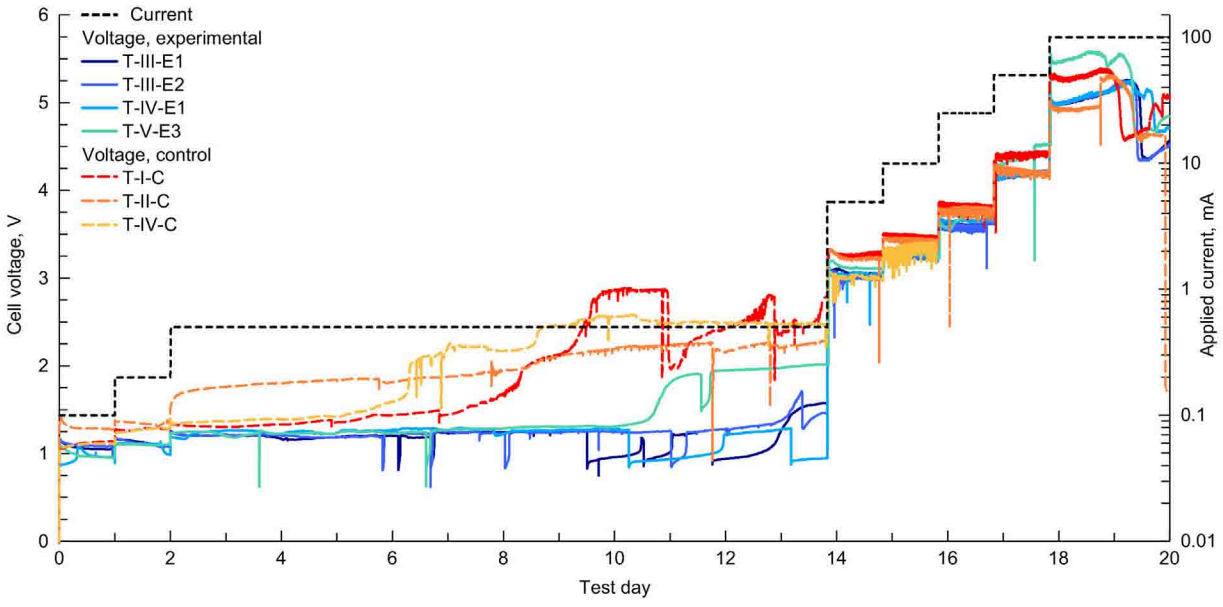

Fig. 5. Cell-applied current (dashed) and resulting cell voltage (solid) over time for several experimental (E) and control (C) cells.

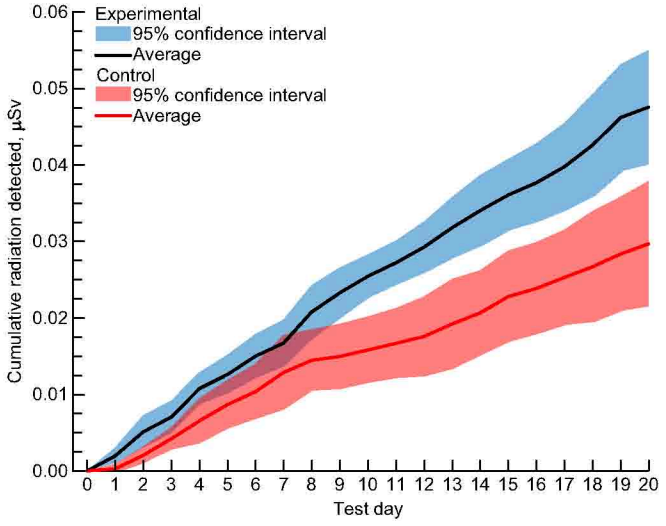

Fig. 7. Average radiation dose detected with 95% confidence intervals for experimental (blue) and control cells (red) over the test duration.

5. Discussion

5.1. Measurement uncertainty

Bubble detectors are designed for bubbles to be manually counted when only low bubble counts exist. The detectors are sized to store greater than 100 distinct bubbles. No scenario in this testing required manual counting of more than 31 bubbles in a single detector. In this range, individual bubbles are easily discernable. Bubble counts are not fractional, and no discrimination is required for identifying what is and what is not a bubble. Additionally, since detectors were infrequently substituted within a trial, any counting error would not carry forward to succeeding counts. To further minimize the effect of counting errors on the measurement, each day the total number of bubbles was counted rather than new bubbles only. Thus, a miscount, such as double counting of a bubble on a given test day, would be reconciled the next test day. In this way, daily bubble counts were independent of previous counting, and overcounting errors (although none were identified) would not affect ongoing measurements.

Bubble detector sensitivity has been shown to be unaffected by storage times and dosages well beyond the requirements of this testing [10]. Manufacturer-calibrated sensitivity, however, may vary from true sensitivity by ±5%. To evaluate the effect of this tolerance in combination with the potential counting errors on the bubble-count results, an adjusted average was calculated that represented a worst case for bubble detector radiation detection. These adjusted averages are the result of first subtracting one bubble from the actual count for every non-zero experimental cell bubble detector reading and adding one bubble to the actual count for every non-zero control cell bubble detector reading. Then, assuming that all experimental cell detectors report too high and all control cell detectors report too low, the average was multiplied by 0.95 for experimental and 1.05 for control cells. Even if such a counting error were made on every measurement, the experimental cell bubble detectors still measured more average cumulative radiation from test day 10 onwards.

5.2. Comparison to cosmic radiation

It is well established that cosmic radiation results in cosmogenic neutrons contributing to background levels. For the United States, the annual average is ~2.8 µSv [17]. It is noted that the annual effective dose of such neutrons varies by location and altitude (dosage doubles with each mile increase in elevation) and ranges from 0.8 to 2 µSv per year at sea level [18]. Relating these levels to the reported experiment, bubble detectors are near 70% in detection efficiency when angled vertically at 90° from a source [12]. This angle corresponds to an overhead source where the detector cap is nearest the source. For the 20-day test duration, that efficiency combined with the annual (365 days) average dose equates to 0.03 to 0.08 µSv. This is the expected range for cosmogenic neutron background radiation. The average control-cell neutron dosage corresponded to the lower end of the spectrum at 0.030 µSv for the 20-day test duration, whereas the experimental-cell average dosage was higher at 0.048 µSv for the 20 days. Because the case-control methodology involved the experimental and control cell pairings running simultaneously, all bubble detectors should record overhead cosmogenic radiation equally. It is thus highly unlikely that the cosmogenic neutrons were the source of the increased neutron activity measured at the experimental cells.

It is plausible that some of the neutrons recorded by the control cell bubble detectors may have originated from experimental cells. Four detectors each were uncapped to record fume hood radiation either while a trial was in process or when no testing was occurring. When cells were operating within the fume hood, the average radiation dose detected was similar to the experimental average, even though the detectors were not adjacent to any particular cell. Without any operational cells present, background dosages were lower, more similar to the control average. This comparison is ultimately inconclusive because of the small sample size, although it hints at the possibility that a true control average may be lower than what is presented here. Many control cells were operated with active experimental cells located to the left and the right of the control. For reference, the cells were spaced at least 8 cm apart.

5.3. Related work

5.3.1. Neutron detection

In 2007, a research group at SRI International constructed cells substantially similar to the cells described here in regards to electrode materials and electrolyte chemistry, though the SRI cells included magnets near the cells [7]. In an attempt to verify the electrochemical behavior was aneutronic, a BF_3 ionizing neutron detector was located near experimental cells as a current was applied: 0.1 mA for several hours at the test outset, then 0.2 mA for the next 22 h before increasing to 0.5 mA for the remainder of the experiment. Some of the cells produced neutron counts an order of magnitude above background.

5.3.2. Dendritic structure significance

During co-deposition, a near-stoichiometric PdD layer is electrolytically deposited on the cathode. As D^+ ions are continuously driven to the cathode, the Pd that remains adhered to it stays in a highly loaded state. It has been hypothesized that this PdD may be important for creating a nuclear active environment [19]. John Bockris and his associates conjectured that a highly dendritic structure, which may form on the cathode, is important to nuclear activity [8]. They claimed an ability to stop tritium production by purposefully disrupting those structures. Additionally, a Bockris group researcher noted dendritic forms emanating from Pd cathodes after prolonged heavy water electrolysis. It was also theorized that there may be metal-solution field strengths of up to 10^9 V/cm at the tips of dendrites. At dendrite tips containing surface states, field enhancement will occur beyond that achieved for surface states on planar faces. As noted in [8], the authors speculate that electrons may be emitted from the dendrite tip into the gas layer, contributing to the ionization of the deuteron then an acceleration of the D^+ ions into other D atoms adsorbed on the dendrite, which results in the nuclear active region. The high concentration of electrons emitted from the dendritic tips may also be contributing to electron screening, thus allowing fusion events to occur. In companion papers, Steinetz et al. [20] and Pines et al. [21] show evidence of DD fusion when subjecting deuterated erbium and titanium to bremsstrahlung radiation, made possible in part by electron screening.

In the experiments described in the current work, there appears to be a correlation between dendritic deposits on cathodes and observed neutron activity. For comparison, post-test images of several experimental cathode cells are presented in Fig. 8 to show the final palladium deposition dendritic

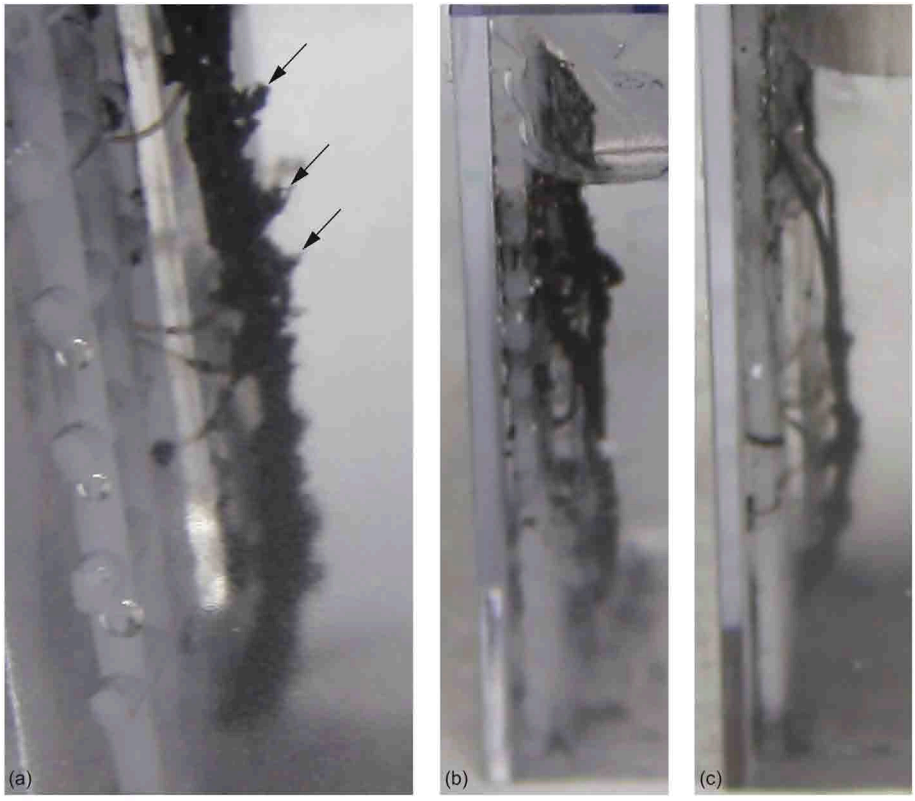

Fig. 8. Close-up images of (a) T-III-E1 (above-average neutron emissions), (b) T-IV-E1 (average neutron emissions), and (c) T-III-E5 (below-average neutron emissions) cathodes prior to post-test disassembly. Note dendritic structure emanating from the cathode, highlighted by several arrows included in (a).

macrostructure on the cathode prior to disassembly. Dendrites are clearly visible on the cathode surface of the T-III-E1 cell, which produced the greatest total neutron dose over 20 days of 0.069 μSV—the greatest of all observed cells. This cell is also notable for the electrolyte clarity and lack of deposits at the bottom of the cell at the end of the test run. Cell T-IV-E1 represents an average neutron-producing experimental cell at 0.043 μSV over 20 days. Although 0.031 μSV over 20 days made T-III-E5 a below-average neutron-producing experimental cell, it was still above the control cell average. It may be that the higher performing cells exhibit more Pd adhering to the cathode surface and a more distinct dendritic structure.

Greater quantities of palladium on the cathode should allow for more reaction surface area. It is unlikely that material on the bottom of the cell contributes to further neutron generation without a mechanism for continued D+ exposure, as it is the current that drives the deposition. Material not in solution or on the electrode effectively becomes removed from the circuit and does not retain deuterium. Regarding expected deuterium loading levels in adhered Pd, Szpak et al. calculated that $PdD_{1.02}$ could form with a 5-mA·cm^{-2} cathodic current density [14], which is similar to the current density achieved in Step 5 of the utilized current profile. Step 5 is also the point in the profile when cell voltage surpasses the thermoneutral voltage for electrolysis of water. The cells start with ~1.7 mol D_2O and ~ 0.16 mol Pd in the cell. Over 20 test days, the cell electrolyzes up to 0.13 mol D_2O, with the majority of that occurring in Step 9. Although Cu is an adequate control analog for Pd, the two elements do not plate out of solution at the same rate, and there is evidence of D_2O decomposition in Pd cells early in the current profile [22]. The higher Cu plating rate is perhaps an explanation for the control cell voltage variability seen in Fig. 5 during test days 2 to 14.

Because of the multiple reactions and phases present in a co-deposition process, it is not simple to calculate relative Pd plating and D loading efficiencies. Furthermore, if dendrites and localized surface reactions are influential, deuterium concentration is unlikely to be uniform. There are many published studies attempting to describe Pd/D electrode loading behavior from first principles and experimental observations [23]. Current density is an input to determining absorption levels and total surface coverage. With all else constant, lower current density can achieve greater absorption and surface coverage levels, even though more time is required to reach steady state. Pd-hydrogen bond strength is higher at the surface layer than in the bulk material and correlates with surface roughness [23,24]. Greater surface roughness means more surface area, suggesting the potential for more deuterium at the surface and greater ability to keep deuterium in bulk Pd in cells with liquid electrolyte. Surface roughness and anodic current density also correspond to enhanced reaction kinetics in Pd/H systems, but there are limits to the potential for improvement [25].

Although all results described in this report derive from the same electrolyte concentrations and current-time profile, other combinations were attempted, producing no definitive neutron generation data. Such null results may merely be due to the probability of observing activity. It is theorized, however, that increasing current too rapidly—early in a test run and prior to significant cathode deposition—does not allow time for the palladium structure to properly form on the cathode surface. Furthermore, simply increasing electrolyte concentration does not guarantee that more material will deposit and remain on the cathode. The dendritic structure and other conditions potentially related to neutron generation are sensitive and characteristically fragile and unstable [26].

5.4. Radiation safety considerations

From the most active experimental cell, T-III-E1, the cumulative dose detected over 56 days was 0.18 μSv. That equates to less than 0.1 μSv per month outside the acrylic vessel. The Occupational Health and Safety Administration (OSHA) whole-body dose limit is 12,500 μSv for a 3-month exposure [27]. Thus, the electrolysis cells present minimal radiation exposure risk compared with OSHA regulations since this testing does not require long-duration exposure during operation. No ongoing alpha, beta, or neutron activity was identified in post-testing analysis of any cell component.

These analysis methods included high-purity germanium (HPGe) gamma scans and Tennelec automated counting for alpha and beta activity.

6. Summary

A case control methodology was followed where a series of experimental and control electrochemical cells were constructed and then monitored with neutron dosimeters in the form of bubble detectors. Bubble detectors offer well-accepted means of measuring neutron activity and give an immediate visual indication of neutron activity. Experimental cells were built using a previously published protocol, which showed prior evidence of neutron activity. These cells consisted of palladium(II) chloride, lithium chloride, and heavy water, with applied currents ranging from 0.1 to 100.0 mA over the test period of 20 days. Control cells were prepared with copper(II) chloride, lithium chloride, and heavy water electrolyte as a means to document background cosmogenic neutron sources, using the same current profile. The bubble detector results provide evidence that there are significantly more neutrons generated by the experimental cells when compared with the control cells. Within a single trial for our standard set-up, the experimental cell exhibited greater neutron production than the adjacent control cell by the end of the run 12 out of 13 times, demonstrating process reproducibility. Based on the bubble detector energy calibration, the neutron energies were greater than 200 keV. Furthermore, from test day 9 through test day 20, the results show that the average cumulative radiation detected near experimental cells exceeds that of control cells at a 99% confidence level ($p < 0.01$).

The findings herein were compared to those of other researchers who found neutron activity using similar cell and operational protocols, but who measured neutron activity with a BF_3 neutron detector. The current work corroborates other research that determined the highest nuclear activity occurred when the PdD deposits resulted in stable dendritic formations on the cathode. In cells where the PdD layer exhibited poor adherence to the electrode, neutron activities were less than the highest neutron-producing cells but still remained above control-cell levels. Even though there is clear evidence of neutron production favoring the experimental cells, the radiation produced by all individual cells was low, and the dose was the equivalent of <0.1 μSv per month adjacent to the cell wall [15].

CRediT authorship contribution statement

Phillip J. Smith: Validation, Formal analysis, Investigation, Resources, Data curation, Writing - original draft, Visualization. **Robert C. Hendricks:** Conceptualization, Methodology, Investigation, Writing - review & editing. **Bruce M. Steinetz:** Conceptualization, Methodology, Writing - review & editing, Supervision, Project administration, Funding acquisition.

Declaration of Competing Interest

None.

Acknowledgments

The authors gratefully acknowledge the assistance of many people that supported this effort. For co-deposition protocol and methodology consultation: Mr. Lawrence Forsley and Dr. Pamela Mosier-Boss; technical support during testing: Mr. Kevin Prokopius; and Statistical support and consultation: Dr. Christopher Daniels. We are also grateful for Dr. Vadim Lvovich (NASA Glenn) for valuable comments on the manuscript; Ms. Laura Becker's patient editorial attention, and Ms. Lorie Passe's careful manuscript preparation. Funding for this work was provided by NASA Headquarters Planetary Sciences Division, Science Mission Directorate.

References

[1] M.C.H. McKubre, F.L. Tanzella, What is needed in LENR/FPE studies? Journal of Condensed Matter Nuclear Science 8 (2012) 187–197.
[2] C.P. Burlinguette, et al., Revisiting the cold case of cold fusion, Nature 570 (2019) 45–51.
[3] N.J.C. Packham, et al., Production of tritium from D_2O electrolysis at a palladium cathode, J. Electroanal. Chem. 270 (1989) 451–458.
[4] P.A. Mosier-Boss, et al., Triple tracks in CR-39 as the result of Pd-D co-deposition: evidence of energetic neutrons, Naturwissenchaften 96 (2009) 135–142.
[5] [Mosier-Boss et al., 2013]. Mosier-Boss PA, et al. (2013). *U.S. Patent No. 8,419,919.* Washington, DC: U.S. Patent and Trademark Office.
[6] P.A. Mosier-Boss, et al., Use of CR-39 in Pd/D co-deposition experiments, The European Physical Journal Applied Physics 40 (2007) 293–303.
[7] F.L. Tanzella, et al., Analysis of the CR-39 detectors from SRI's SPAWAR/Galileo type electrolysis experiments #7 and #5. Signature of possible neutron emission, Proceedings of 8th International Workshop on Anomalies in Hydrogen/Deuterium Loaded Metals 2007, pp. 182–203.
[8] G.H. Lin, et al., Electrochemical fusion: a mechanism speculation, J. Electroanal. Chem. 280 (1990) 207–211.
[9] Bubble Technology Industries, Personal Neutron Dosimeters Data Sheet, http://bubbletech.ca/wp-content/uploads/2014/02/BTI_BUBBLE_General_May720091.pdf 2009 accessed 24 August 2020.
[10] H. Ing, Bubble detectors—a maturing technology, Radiat. Meas. 27 (1997) 1–11.
[11] M.B. Smith, et al., Bubble-detector measurements of neutron radiation in the international Space Station, Radiat. Prot. Dosim. 168 (2016) 154–166.
[12] H. Ing, Neutron measurements using bubble detectors—terrestrial and space, Radiat. Meas. 33 (2001) 275–286.
[13] P.A. Mosier-Boss, et al., Investigation of nano-nuclear reactions in condensed matter, Defense Threat Reduction Agency (2016) 1–104.
[14] S. Szpak, et al., Deuterium uptake during Pd-D co-deposition, J. Electroanal. Chem. 379 (1994) 121–127.
[15] P.A. Mosier-Boss, et al., Detection of high energy particles using CR-39 detectors part 1: results of microscopic examination, scanning, and LET analysis, Int. J. Hydrog. Energy 42 (2017) 416–428.
[16] T.W. Anderson, D.A. Darling, A test of goodness-of-fit, American Statistical Association Journal 49 (1954) 765–769.
[17] J.T. Voss, Los Alamos Radiation Monitoring Notebook, United States Department of Energy Los Alamos National Laboratory, Los Alamos, NM, 2001.
[18] C.W. Jameson, et al., Report on Carcinogens Background Document for X Radiation & Gamma Radiation and Neutrons, Technology Planning and Management Corporation for U.S. Department of Health and Human Services Public Health Service National Toxicology Program, Durham, NC, 2003.
[19] E. Storms, The Science of Low Energy Nuclear Reaction: A Comprehensive Compilation of Evidence and Explanations about Cold Fusion World Scientific Publishing Company, 2007.
[20] Steinetz BM, et al. (2020). "Novel nuclear reactions observed in bremsstrahlung-irradiated deuterated metals," *Phys. Rev. C 101 (NASA/TP-2020-5001616)*, 044610. https://doi.org/10.1103/PhysRevC.101.044610 [accessed 24 August 2020].
[21] Pines V, et al. (2020). Nuclear fusion reactions in Deuterated metals , *Phys. Rev. C 101 (NASA/TP—2020-5001617)*, 044609. https://doi.org/10.1103/PhysRevC.101.044609 [accessed 24 August 2020].
[22] P.A. Mosier-Boss, L.P. Forsley, Energetic Particle Emission in Pd/D co-Deposition: An Undergraduate Research Project to Replicate a New Scientific Phenomenon, Journal of Laboratory Chemical Education 6 (2018) 69–76.
[23] S.J. Szpak, P.A. Mosier-Boss, "Anomalous behavior of the Pd/D system," Naval Command, Control, and Ocean Surveillance Center/TR1696, 1995.
[24] R.V. Bucur, F. Bota, Transfer equilibrium in the surface layer of a (Pd-H)-electrode with low hydrogen content, Electrochemica Acta 29 (1984) 103–106.
[25] R.V. Bucur, F. Bota, Galvanostatic desoption of hydrogen from Pd layers–III. The anodic Volmer reaction, Electrochemica Acta 28 (1983) 1373–1378.
[26] Y.E. Kim, Surface reaction mechanism for deuterium-deuterium fusion with a gas/solid-state fusion device, Fusion Technology 19 (1991) 558.
[27] Occupational Safety and Health Administration (2019). "Introduction to ionizing radiation," United States Department of Labor. https://www.osha.gov/SLTC/radiationionizing/introtoionizing/ionizinghandout.html [accessed 4 November 2019].